Antoinette Maniatty[1]
Professor
Fellow ASME
Department of Mechanical, Aerospace, and Nuclear Engineering,
Rensselaer Polytechnic Institute,
Troy, NY 12180-3590
e-mail: maniaa@rpi.edu

Payman Karvani
Mem. ASME
Department of Mechanical, Aerospace, and Nuclear Engineering,
Rensselaer Polytechnic Institute,
Troy, NY 12180-3590
e-mail: paymaan@gmail.com

Constitutive Relations for Modeling Single Crystal GaN at Elevated Temperatures

Thermal–mechanical constitutive relations for bulk, single-crystal, wurtzite gallium nitride (GaN) at elevated temperatures, suitable for modeling crystal growth processes, are presented. A crystal plasticity model that considers slip and the evolution of mobile and immobile dislocation densities on the prismatic and basal slip systems is developed. The experimental stress–strain data from Yonenaga and Motoki (2001, "Yield Strength and Dislocation Mobility in Plastically Deformed Bulk Single-Crystal GaN," J. Appl. Phys., ***90****(12), pp. 6539–6541) for GaN is analyzed in detail and used to define model parameters for prismatic slip. The sensitivity to the model parameters is discussed and ranges for parameters are given. Estimates for basal slip are also provided.* [DOI: 10.1115/1.4028441]

1 Introduction

GaN, a member of the III-nitrides, possesses some excellent properties including a wide band gap, low thermal expansion, high thermal conductivity, and high melting point, making it valuable for the fabrication of high power transistors and high frequency opto-electronic devices, such as light emitting diodes and laser diodes [1,2]. GaN may either have a zinc-blende (cubic) or a wurtzite (hexagonal) structure, with the wurtzite form being the most common and thus, the focus of this work.

Currently, the production cost of free-standing GaN substrates remains high because they are difficult to produce. The two leading approaches to making bulk GaN are hydride vapor phase epitaxy (HVPE) and ammonothermal growth. At present, the dominant bulk growth process is HVPE [3,4]. Due to the thermal and lattice mismatch stresses generated within the crystal during the growth process, production is limited by stress-induced cracks and defects, primarily in the form of dislocations, which limit the performance and lifetime of the devices. The dislocation density in HVPE grown GaN is typically 10^6–$10^8\,\mathrm{cm}^{-2}$, with the dislocation density decreasing as the GaN layer thickness increases [5]. However, thicker layers have a greater probability of cracking. The ammonothermal growth process, utilizing a solution/reaction mechanism, shows promise in producing bulk GaN crystals with better structural properties, including lower dislocation density (reported as low as $5 \times 10^3\,\mathrm{cm}^{-2}$) [6–8]. Understanding and modeling the thermal–mechanical behavior of single crystal GaN under growth conditions can be used to accelerate improvements in process design to allow for more efficient production of high quality crystals.

While the opto-electrical properties of GaN are well characterized, less is known about the thermal–mechanical behavior of GaN, especially at elevated temperatures. Information on thermal–mechanical properties at elevated temperature is crucial for controlling plastic deformation and dislocation formation during crystal growth and device processing and also to improve the opto-electrical properties of the material [9]. For thermal–mechanical analysis, it is necessary to characterize the temperature dependent thermal expansion, linear elastic response, and plastic response. While measurements and estimates of the temperature dependent thermal expansion coefficients and elastic moduli have been made for GaN, the yield and plastic behavior is more difficult to characterize.

The thermal–elastic behavior of GaN is fairly well characterized. Leszczynski et al. [10] measured the temperature dependent thermal expansion coefficients in GaN for the temperature range 294–753 K. The thermal expansion coefficients have also been estimated for a much wider range of temperatures (25–1800 K) by Reeber and Wang [11] using a semi-empirical approach and by Wang et al. [12] with a first-principle approach using the density function perturbation theory. Likewise, the elastic moduli have been measured over a temperature range of 100–700 K by Yadav and Pandey [13], and Reeber and Wang [14] estimate the moduli over a broader temperature range (0–900 K) empirically from corresponding state relationships and data from other hexagonal Grimm–Sommerfeld compounds.

The plastic behavior is associated with the underlying phenomena of dislocation glide on the slip systems and dislocation multiplication and interactions, making it more difficult to model and characterize. The plastic behavior of GaN films has been studied primarily through indentation tests [15–17]. However, indentation tests are difficult to interpret because they produce a complex stress field below the indenter and induce slip on multiple slip systems [18]. Yonenaga and Motoki [9] performed compression tests on bulk single crystal GaN at temperatures of 900, 950, and 1000 °C. Those tests were oriented for single slip on the $[11\bar{2}0](1\bar{1}00)$ prismatic slip system. Recently, Wheeler et al. [19] performed compression tests on {0001}-oriented GaN micropillars in situ in a scanning electron microscope at temperatures up to 479.3 °C. Deformation was observed on the $< 11\bar{2}3 > \{11\bar{2}2\}$ pyramidal slip system. Strain rate jump tests were also performed to determine the strain rate sensitivity.

Constitutive models to describe the plastic behavior of semiconductor single crystals are generally based on the model developed by Alexander and Haasen [20] for elemental semiconductors loaded in a single slip orientation. That model relates the plastic deformation in the crystal to the movement and multiplication of dislocations and assumes a power law relating the resolved shear stress and the dislocation velocity. Yonenaga and coworkers have used a modified form of the original Alexander and Haasen model to describe the single slip plastic behavior of elemental semiconductors [21], III–V compounds [22], and GaN [9]. Wheeler et al. [19] use a hyperbolic sine model to relate the shear flow stress and dislocation velocity for pyramidal slip in GaN, which is based on the model for steady-state creep first proposed by Garofalo [23]. Crystal plasticity models that extend the single slip models to consider multislip in cubic crystal semiconductors have been developed by Moosbrugger [24] for CdTe, by Kalan and Maniatty [25] for InP, and by Zhang and coworkers [26] for Si.

In this paper, a framework for thermal–elastic–viscoplastic modeling of wurtzite GaN is outlined, and a new crystal plasticity

[1]Corresponding author.
Contributed by the Materials Division of ASME for publication in the Journal of Engineering Materials and Technology. Manuscript received April 28, 2014; final manuscript received August 8, 2014; published online September 24, 2014. Assoc. Editor: Irene Beyerlein.

Copyright © 2015 by ASME

Downloaded From: http://materialstechnology.asmedigitalcollection.asme.org/ on 03/17/2016 Terms of Use: http://www.asme.org/about-asme/terms-of-use

constitutive model is presented. The model considers the hexagonal crystal structure, slip on the prismatic and basal slip systems, and the evolution of mobile and immobile dislocation densities. Model parameters for prismatic slip are determined after a detailed analysis of the GaN compression test data of Yonenaga and Motoki [9]. Model parameter estimates for basal slip are also provided. The sensitivity to the model parameters is discussed. The model is suitable for modeling the thermal–mechanical behavior of GaN under growth conditions for use in process design. The constitutive framework may also be extended to other wurtzite crystals, such as AlN.

2 Thermal–Mechanical Model Formulation

During crystal growth, due to the thermal–mechanical loads, the crystal will deform thermally, elastically, and plastically. Thus, the crystal strain, assuming small strains and using standard indicial notation [27], may be expressed as

$$\varepsilon_{ij} = \varepsilon^{\theta}_{ij} + \varepsilon^{e}_{ij} + \varepsilon^{p}_{ij} \tag{1}$$

where superscripts θ, e, and p refer to the thermal, elastic, and plastic parts of the strain, respectively.

The thermal strain depends only on the change in temperature through the following relationship:

$$\varepsilon^{\theta}_{ij} = \int_{\theta_o}^{\theta_f} \alpha_{ij}(\theta)d\theta, \quad \alpha_{ij} = R_{ik}\bar{\alpha}_{kl}R_{jl} \tag{2}$$

where α_{ij} and $\bar{\alpha}_{kl}$ are the temperature dependent components of the thermal expansion tensor with respect to the global and lattice reference frames, respectively, and θ_o and θ_f are the initial and final temperatures. The second equation in Eq. (2) represents the rotation from the lattice to the global reference frame. Since GaN has hexagonal crystal symmetry, letting the $\bar{x}_3$ axis be aligned with the crystal c axis in the lattice frame (denoted by overbar), the only nonzero components of the thermal expansion tensor are $\bar{\alpha}_{11} = \bar{\alpha}_{22} = \alpha_a$ and $\bar{\alpha}_{33} = \alpha_c$, where α_a and α_c are the thermal expansion coefficients along the crystal a and c directions.

The elastic strain is linearly related to the stress, σ_{ij}, at a given temperature

$$\sigma_{ij} = \mathcal{C}_{ijkl}(\theta)\varepsilon^{e}_{kl}, \quad \mathcal{C}_{ijkl} = R_{im}R_{jn}R_{kp}R_{lq}\bar{\mathcal{C}}_{mnpq} \tag{3}$$

where $\mathcal{C}_{ijkl}$ are the temperature dependent components of the fourth-order elasticity tensor with respect to the global reference frame. For hexagonal symmetry, there are only five independent components of $\bar{\mathcal{C}}_{ijkl}$ with respect to the lattice frame. Using the standard contracted notation (see, for example, Bower [27]), these five independent elastic stiffness components are $\bar{C}_{11}, \bar{C}_{33}, \bar{C}_{12}, \bar{C}_{13}$, and $\bar{C}_{44}$. Yadav and Pandey [13] measured the elastic moduli over a temperature range of 100–700 K and Reeber and Wang [14] estimated the moduli over the range 0–900 K. Those results are in fairly good agreement except for the parameter $\bar{C}_{12}$. In this work, the experimental data of Yadav and Pandey is fit to quadratic curves yielding

$$\bar{C}_{11} = 385.54 - 9.3809 \times 10^{-3}\theta - 1.2381 \times 10^{-5}\theta^2 \tag{4}$$

$$\bar{C}_{33} = 387.99 - 9.0119 \times 10^{-3}\theta - 1.2976 \times 10^{-5}\theta^2 \tag{5}$$

$$\bar{C}_{12} = 94.671 - 2.1786 \times 10^{-3}\theta - 3.2143 \times 10^{-6}\theta^2 \tag{6}$$

$$\bar{C}_{13} = 81.414 - 1.5357 \times 10^{-3}\theta - 3.2143 \times 10^{-6}\theta^2 \tag{7}$$

$$\bar{C}_{44} = 97.714 - 2.2500 \times 10^{-3}\theta - 3.2143 \times 10^{-6}\theta^2 \tag{8}$$

where θ is the temperature in K and the elastic parameters are in GPa.

The plastic strain ε^{p}_{ij} depends on the history of the stress and temperature, and is considerably more complex to model as it is associated with the micromechanical mechanism of dislocation motion on crystallographic slip systems and the evolution of dislocation density. The formulation of the crystal plasticity model proposed here is discussed in Sec. 3.

3 Crystal Plasticity Model

In order to accurately model the plastic behavior of GaN crystals at elevated temperatures, it is necessary to define a crystal plasticity model that is capable of capturing the underlying effects of dislocation motion, multiplication, and interactions. In this work, we modify and expand the model originally developed by Alexander and Haasen [20]. The Alexander and Haasen model is a micromechanical (dislocation dynamical) constitutive model that relates plastic deformation on a single slip system in crystals with a diamond structure to the motion and multiplication of dislocations. Here, we first present a modified form of this model for single slip in GaN. Next, we expand the model to consider slip on multiple slip systems in GaN crystals with a wurtzite structure and link the plastic strain to the stress.

3.1 Single Slip Model. The model starts with the Orowan equation [28], which relates the rate of plastic shear, $\dot{\gamma}$, on the slip system to the dislocation motion

$$\dot{\gamma} = \rho_m b v \tag{9}$$

where ρ_m is the mobile dislocation density, b is the magnitude of the Burgers vector, and v is the average dislocation velocity. At temperatures above $0.4\,T_m$, where T_m is the melt temperature, dislocation glide-controlled power-law creep behavior is expected [29]. The melt temperature of GaN, under high pressure, has been found to be approximately $T_m = 2200$ K [30], and thus, at temperatures above 880 K (610 °C), the dislocation velocity may be expressed in terms of the resolved shear stress τ on the slip system as

$$v = v_o \exp\left(\frac{-Q}{k\theta}\right)\left(\frac{< \tau - \hat{\tau} >}{\tau_o}\right)^n \tag{10}$$

where $\hat{\tau}$ is a shear stress that needs to be overcome to initiate glide ($<x> = 0$ if $x < 0$, $<x> = x$ if $x > 0$), n is the inverse of the empirical strain rate sensitivity, Q is the activation energy for dislocation glide, k is Boltzmann's constant, and τ_o and v_o are constant reference stress and dislocation velocity, respectively. The stress needed to initiate slip, $\hat{\tau}$, is assumed to have two parts, a constant friction stress, $\hat{\tau}_f$, representing the resistance of the crystal lattice to dislocation movement, and a strain hardening term associated with the dislocation–dislocation interactions

$$\hat{\tau} = \hat{\tau}_f + f\,Gb\sqrt{\rho_f} \tag{11}$$

where ρ_f is the immobile dislocation density, f is a coefficient typically taken as one-third, and G is the elastic shear modulus. Eqs. (9)–(11) are identical to those proposed by Alexander and Haasen [20], with the following two exceptions: (a) the mobile, ρ_m, and immobile, ρ_f, dislocation densities are separated here, where Alexander and Haasen assumed a single dislocation density and (b) a friction stress, $\hat{\tau}_f$, is added to the stress needed to initiate slip in this work.

In addition to the power law relation in Eq. (10), we also consider a power law similar to that frequently used to model viscoplasticity in metals at elevated temperatures [31,32]

$$v = v_o \exp\left(\frac{-Q}{k\theta}\right)\left(\frac{\tau}{\hat{\tau}}\right)^n \tag{12}$$

Finally, evolution equations for the mobile and immobile dislocation densities are needed. Johnston and Gilman [33] proposed

Downloaded From: http://materialstechnology.asmedigitalcollection.asme.org/ on 03/17/2016 Terms of Use: http://www.asme.org/about-asme/terms-of-use

that the multiplication of mobile dislocations occurs proportionally to their length and the distance traveled, and thus

$$\dot{\rho}_{\mathrm{m}} = \delta \rho_{\mathrm{m}} v = \frac{\delta}{b}\dot{\gamma} \tag{13}$$

where δ is the number of dislocations generated per distance moved, and Eq. (9) is used above to obtain the second relation. Dew-Hughes [34] assumed δ to be constant, whereas Peissker et al. [35] postulated that δ was proportional to the effective shear stress, $\tau_{\mathrm{eff}} = \tau - \hat{\tau}$. Here, we use dislocation density evolution equations similar to those proposed by Kubin and Estrin [36], who assume δ is constant and also include the immobilization of mobile dislocations being trapped by other mobile and immobile dislocations. Specifically, we assume evolution equations of the form

$$\dot{\rho}_{\mathrm{m}} = \left[\frac{g_1}{b^2} - g_2 \rho_{\mathrm{m}} - \frac{g_3}{b}\sqrt{\rho_f}\right]\dot{\gamma} \tag{14}$$

$$\dot{\rho}_f = \left[g_2 \rho_{\mathrm{m}} + \frac{g_3}{b}\sqrt{\rho_f} - g_4 \exp\left(-\frac{Q_{\mathrm{v}}}{k\theta}\right)\rho_f\right]\dot{\gamma} \tag{15}$$

where g_1–g_4 are dimensionless constants. The first term in Eq. (14) is the dislocation multiplication term ($\delta = g_1/b$), and the last two terms are associated with the trapping of mobile dislocations by other mobile and immobile dislocations. Those immobilized dislocations then appear as the first two terms in Eq. (15), with the last term in that equation associated with thermally activated recovery, where Q_{v} is the activation energy for lattice diffusion.

3.2 Extension to Multislip.

The primary slip systems for GaN are the prismatic $< 11\bar{2}0 > \{1\bar{1}00\}$ and basal $< 11\bar{2}0 > (0001)$ systems. Under highly constrained loading conditions, slip is sometimes observed on the $< 11\bar{2}3 > \{11\bar{2}2\}$ and $< 11\bar{2}0 > \{1\bar{1}01\}$ pyramidal slip systems, such as in the micropillar tests of Wheeler et al. [19] where the loading was such that no significant shear stress was applied on the basal and prismatic slip systems, or in nano-indentation tests [37]. However, the stress required to move a dislocation on the pyramidal slip systems is significantly higher than that on either the basal or prismatic slip systems, as was shown using molecular dynamics simulations recently for the $< 11\bar{2}0 > \{1\bar{1}01\}$ system [38]. Furthermore, under normal growth conditions, dislocations are observed only on the prismatic and basal slip planes [39,40]. Thus, in this work, we consider only the three prismatic and three basal slip systems, but the model can be extended to include pyramidal slip systems as well.

The multislip model starts by assuming that plastic deformation is due to slip on crystallographic slip systems such that the plastic strain rate may be expressed as

$$\dot{\varepsilon}^p_{ij} = \sum_{\alpha=1}^{n_s} \dot{\gamma}^\alpha S^\alpha_{ij}, \qquad S^\alpha_{ij} = \frac{1}{2}R_{ik}\left(\bar{s}^\alpha_k \bar{m}^\alpha_l + \bar{s}^\alpha_l \bar{m}^\alpha_k\right)R_{jl} \tag{16}$$

where $\dot{\gamma}^\alpha$ is the rate of plastic shearing on the α system, $n_{\mathrm{s}} = 6$ is the number of slip systems, S^α_{ij} is the symmetric part of the Schmid tensor with respect to the global reference frame, $\bar{s}^\alpha_k$ and $\bar{m}^\alpha_l$ are the slip direction and the slip plane normal for the α slip system with respect to the lattice reference frame. During deformation, the material may rotate as well as strain. The rate of small rotations is

$$\dot{w}_{ij} = \dot{R}_{ik}R_{jk} + \dot{w}^p_{ij}, \quad \dot{w}^p_{ij} = \sum_{\alpha=1}^{n_s}\dot{\gamma}^\alpha A^\alpha_{ij}$$
$$A^\alpha_{ij} = \frac{1}{2}R_{ik}\left(\bar{s}^\alpha_k \bar{m}^\alpha_l - \bar{s}^\alpha_l \bar{m}^\alpha_k\right)R_{jl} \tag{17}$$

where $\dot{w}^p_{ij}$ is the plastic spin due to slip.

The driving force causing slip deformation is the shear stress along the slip direction on the slip plane. The resolved shear stress on slip system α can be expressed as

$$\tau^\alpha = \sigma_{ij} S^\alpha_{ij} \tag{18}$$

The remainder of the model is an extension of the single slip model to the multislip case. Equations (9)–(12) can be combined into an expression defined for each slip system as

$$\dot{\gamma}^\alpha = \rho^t_{\mathrm{m}} b v_{\mathrm{o}} \exp\left(\frac{-Q^t}{k\theta}\right)(\tau^\alpha_{\mathrm{d}})^n \mathrm{sgn}(\tau^\alpha) \tag{19}$$

where superscript t is introduced to differentiate prismatic ($t = p$) and basal ($t = b$) slip systems, $\mathrm{sgn}(\tau^\alpha)$ takes the sign of τ^α to ensure that $\dot{\gamma}^\alpha$ and τ^α are in the same direction, and τ^α_{d} represents a generalized dimensionless shear stress such that

$$\tau^\alpha_{\mathrm{d}} = \frac{< |\tau^\alpha| - \hat{\tau}^t >}{\tau_{\mathrm{o}}} \tag{20}$$

or

$$\tau^\alpha_{\mathrm{d}} = \frac{|\tau^\alpha|}{\hat{\tau}^t} \tag{21}$$

depending on which power law relation is used. The stress needed to initiate slip is expected to be different on the basal and prismatic slip systems, but is assumed to be the same on all slip systems of the same type t, and is expressed as

$$\hat{\tau}^t = \hat{\tau}^t_f + f\, G^t b\sqrt{\rho^t_f} \tag{22}$$

where $G^b = \bar{C}_{44}$ for basal slip and $G^p = \bar{C}_{66} = \frac{1}{2}(\bar{C}_{11} - \bar{C}_{12})$ for prismatic slip. Adopting a framework similar to thats proposed by Beyerlein and Tomé [41] for Zr, which also has a hexagonal crystal structure, we assume evolution equations for the dislocation densities on the basal and prismatic slip systems of the form

$$\dot{\rho}^t_{\mathrm{m}} = \left[\frac{g^t_1}{b^2} - g^t_2 \rho^t_{\mathrm{m}} - \frac{g^t_3}{b}\sqrt{\rho^t_f}\right]\dot{\gamma}^t \tag{23}$$

$$\dot{\rho}^t_f = \left[g^t_2 \rho^t_{\mathrm{m}} + \frac{g^t_3}{b}\sqrt{\rho^t_f} - g^t_4 \exp\left(-\frac{Q_v}{k\theta}\right)\rho^t_f\right]\dot{\gamma}^t \tag{24}$$

$$\dot{\gamma}^t = \sum_{\alpha\in t}|\dot{\gamma}^\alpha| \tag{25}$$

where Eq. (25) indicates summation over the slip systems α that are in type t of the shear rates.

To estimate the material parameters in the proposed model, we focus on the experimental data for single slip on the prismatic slip systems presented in Yonenaga and Motoki [9]. We start with a detailed study of the data presented in Yonenaga and Motoki to determine parameters for the prismatic slip systems. Then, using the results of the molecular dynamics dislocation mobility study by Weingarten and Chung [38], we estimate parameters for basal slip.

4 Prismatic Single Slip Data Analysis

The stress–strain response of GaN at elevated temperatures was first measured by Yonenaga and Motoki [9] using a uni-axial compression deformation experiment on single crystal GaN oriented for single slip on a prismatic slip system. Specifically, the $[11\bar{2}0](1\bar{1}00)$ slip system was inclined by 45 deg from the compression axis. Tests were performed at temperatures of 900, 950, and 1000 °C. The authors report an applied macroscopic shear

Downloaded From: http://materialstechnology.asmedigitalcollection.asme.org/ on 03/17/2016 Terms of Use: http://www.asme.org/about-asme/terms-of-use

strain rate of 4.5×10^{-4} s^{-1}. However, since it was a compression test, a compressive strain rate must have been applied, and the authors deduced the reported shear strain rate on the prismatic slip system.

Figure 1 shows a diagram of the oriented crystal sample, where the lattice coordinates $\bar{x}_1$ and $\bar{x}_2$ are aligned with the slip direction $[11\bar{2}0]$ and opposite the slip plane normal direction $(1\bar{1}00)$. For single slip and using Eqs. (16) and (18), we obtain relations for the applied compressive plastic strain rate and stress in terms of the shear strain rate and resolved shear stress

$$|\dot{\varepsilon}^p_{22}| = |\dot{\gamma} S_{22}| = \frac{1}{2}|\dot{\gamma}| \tag{26}$$

$$|\tau| = |S_{22}\sigma_{22}| = \frac{1}{2}|\sigma_{22}| \tag{27}$$

Figure 2 shows plots of the data reported in Yonenaga and Motoki [9], where the bottom and left scale are apparent shear strain, γ^{app}, and resolved shear stress, τ, respectively. Here, we add the top and right scale, which we assume to be the actual applied apparent compressive strain, $\varepsilon^{\mathrm{app}} = -\varepsilon^{\mathrm{app}}_{22}$, and measured compressive stress, $\sigma = -\sigma_{22}$, where

$$\varepsilon^{\mathrm{app}} = \frac{1}{2}\gamma^{\mathrm{app}} \quad \text{and} \quad \sigma = 2\tau \tag{28}$$

based on Eqs. (26) and (27), where the apparent applied compressive strain is equated to the plastic compressive strain assuming negligible elastic strains [42]. The stress–strain curves at all temperatures are characterized by an apparent elastic increase in the stress, a smooth yield behavior, and a subsequent gradual increase in the stress with strain.

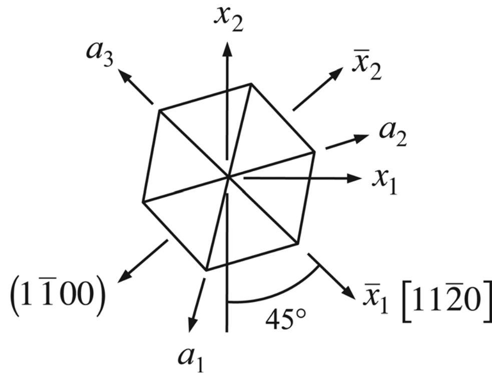

Fig. 1 Orientation of the GaN hexagonal lattice relative to the compression experiment, where the x_1, x_2 are coordinates of the global reference frame with x_2 aligned with the compressive axis, and $\bar{x}_1$, $\bar{x}_2$ are the lattice reference frame coordinates

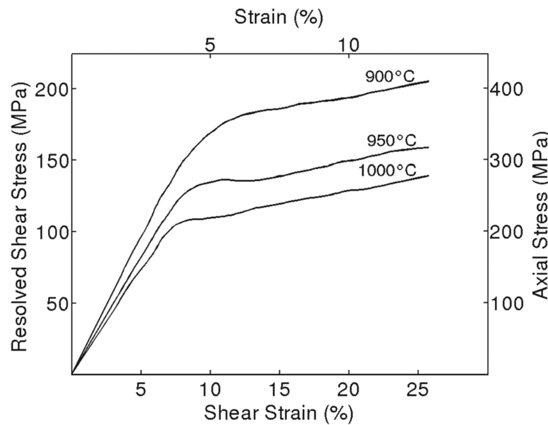

Fig. 2 Stress–strain curves of GaN bulk single crystals, based on data from Yonenaga and Motoki [9]

A significant stress drop in the yield region, which is typical for various elemental and compound semiconductors, such as Si [43] and InP [44,45], is not observed for GaN in these tests. While the stress drop is found to be reduced or to disappear in other semiconductors when the initial dislocation density is relatively high (above 10^6 cm^{-2}) [43], at higher temperatures [44], and at lower strain rates [45], the conditions here are comparable to those where a stress drop is observed. Specifically, the initial dislocation density in the GaN sample was reported to be about 10^5 cm^{-2}. The homologous temperatures of the tests are in the range of $T_{\mathrm{h}} = 0.42$–0.46, which is a lower homologous temperature range than that studied in Yonenaga and Sumino [44] for InP, where substantial yield stress drops were observed with a comparable strain rate on the order of 10^{-4} s^{-1}. It is interesting to note that a stress drop was also not observed in similar compression tests on 6H-SiC, another semiconductor with a wurtzite structure that was oriented for single slip on the basal plane [46].

For the linear, presumably elastic, part of uni-axial stress–strain curves in Fig. 2, the slopes are in the range of 6000–8000 MPa. The linear elastic region should have a slope equal to the elastic modulus for the given orientation, which for GaN at the temperatures tested is in the range of 320–330 GPa. The observed reduced slope is typically attributed to machine compliance [24,33], that is, not only is the crystal deforming, but because the crystal is very stiff relative to the testing machine, the testing machine is also deforming. To correct the data for machine compliance, the compliance of the testing machine is modeled as a spring (linear elastic material) in series with the test specimen, because data shows linear loading curves. Letting ε^m and ε^e be the compressive machine and elastic strains in the sample, then

$$\varepsilon^{\mathrm{app}} = \varepsilon^m + \varepsilon^e = \frac{\sigma}{E_{\mathrm{m}}} + \frac{\sigma}{E_{\mathrm{s}}} \tag{29}$$

where E_{m} is the effective elastic modulus of the machine, and E_{s}, the elastic modulus of the GaN sample, which for the given orientation is

$$E_{\mathrm{s}} = \frac{\bar{C}_{33}(\bar{C}^2_{11} - \bar{C}^2_{12}) - 2\bar{C}^2_{13}(\bar{C}_{11} - \bar{C}_{12})}{\bar{C}_{11}\bar{C}_{33} - \bar{C}^2_{13}} \tag{30}$$

Using the linear part of the data from each curve, we obtain approximate values for E_{m} of 7800, 6600, and 5900 MPa at 900, 950, and 1000 °C, respectively. The machine compliance strain may now be removed from the strain data, specifically the true compressive strain in the sample ε is

$$\varepsilon = \varepsilon^{\mathrm{app}} - \varepsilon^m = \varepsilon^{\mathrm{app}} - \frac{\sigma}{E_{\mathrm{m}}} \tag{31}$$

where the machine is assumed to remain linear elastic throughout the test. Stress–strain curves corrected for machine compliance are shown in Fig. 3.

The plastic strain and strain rate may also be computed now. The compressive plastic strain is computed using Eq. (1)

$$\varepsilon^p = \varepsilon - \varepsilon^e = \varepsilon - \frac{\sigma}{E_{\mathrm{s}}} \tag{32}$$

For each point along the original experimental curves in Fig. 2, we know $\gamma^{\mathrm{app}} = \dot{\gamma}^{\mathrm{app}} t = (4.5 \times 10^{-4}\ \mathrm{s}^{-1})t$, and, thus, we know the time, t, for each data point. Using the averaging method in Anderssen and Hegland [47], which allows the stable computation of low order derivatives from observational data, we compute the compressive plastic strain rate, $\dot{\varepsilon}^p$. For the single slip geometry, using Eq. (26), we may then find the plastic shear rate, $\dot{\gamma} = 2\dot{\varepsilon}^p$, which is plotted in Fig. 4 against the plastic shear strain. It is

Downloaded From: http://materialstechnology.asmedigitalcollection.asme.org/ on 03/17/2016 Terms of Use: http://www.asme.org/about-asme/terms-of-use

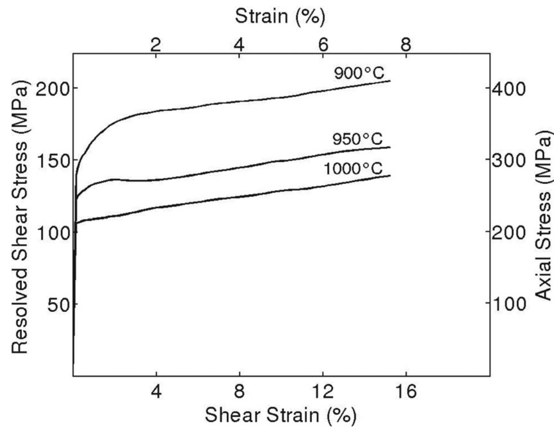

Fig. 3 Stress–strain curves of GaN bulk single crystals at temperatures of 900, 950, and 1000 °C, based on data from Yonenaga and Motoki [9], corrected for machine compliance

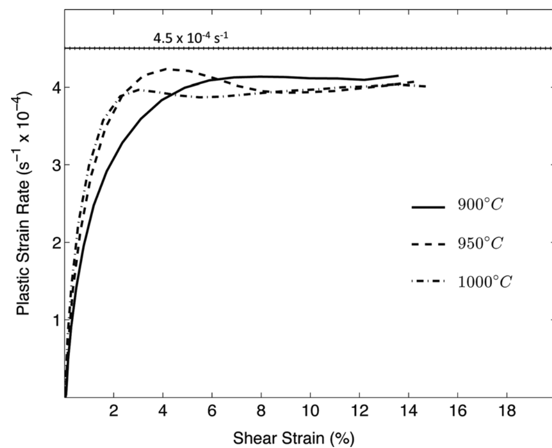

Fig. 4 Computed plastic strain rate for Yonenaga and Motoki [9] experiment at temperatures of 900, 950, and 1000 °C

interesting to note that the rate of shearing on the slip system is evolving over a substantial part of the test and never reaches the apparent applied rate of 4.5×10^{-4} s^{-1} due to continued hardening. Since the plastic strain rate is changing, the data contain information on the rate sensitivity, which would not be available if the data were for a uniform strain rate.

5 Model Parameters

We can use the preceding analysis of the Yonenaga and Motoki [9] data to fit the model parameters for prismatic slip, $t = p$, in Eqs. (19)–(25). The magnitude of the Burgers vector for GaN in both prismatic and basal slip is $b = 3.2$ Å, and we assume the initial mobile and immobile dislocation densities are $\rho_{m0} = \rho_{f0} = 10^9\,\mathrm{m}^{-2}$, equal to the reported initial dislocation density. We also assume a reference shear stress of $\tau_o = 1$ MPa and coefficient $f = 1/3$. Since the hardening curves do not appear to be saturating, the last term in Eq. (24) does not appear to have an effect, and thus g_4 cannot be determined.

This leaves seven parameters to be determined for modeling prismatic slip, v_o, Q^p, n, $\hat{\tau}_f^p$, g_1^p, g_2^p, and g_3^p. The first four of these parameters are associated with the temperature dependent dislocation glide behavior, and the last three are primarily associated with the hardening behavior. Since we do not see a significant stress drop, which is associated with a rapid growth in the mobile dislocation density post-yield, it is reasonable to assume limited growth in the mobile dislocation density. We first estimate the four parameters, v_o, Q^p, n, $\hat{\tau}_f^p$, by fitting the data without evolving the dislocation densities. Next, we estimate g_1^p, g_2^p, and g_3^p allowing the dislocation densities to evolve, and refine all the other parameters to best match the data.

There is not a unique set of parameters that provides a good fit to the data. The results are least sensitive to v_o. Two extreme cases of parameters that lead to a good fit of the shear stress–strain data to within a root-mean-square deviation (RMSD) in the shear stress of 7 MPa, where Eq. (20) is used in the power law, are give in Table 1. We find $\hat{\tau}_f = 44.7 \pm 0.6$ MPa, and while both Q^p and n increase with v_o, $Q^p/n = 1.00 \pm 0.03$. The optimal fit for all the parameters, setting $v_o = 10^3$ m/s and considering both forms for the power law (Eqs. (20) and (21)), are listed in Table 2 and plotted in Fig. 5. The RMSD in the shear stress is 5 MPa when Eq. (20) is used and is 13 MPa when Eq. (21) is used. Thus, the model with Eq. (20) provides a better fit to the data. The evolution of the mobile and immobile dislocation densities, assuming the model with Eq. (20), is shown in Fig. 6. We see that the mobile dislocation density grows rapidly and then saturates, while the immobile dislocation density continues to grow, which leads to the observed hardening behavior. Dislocation data after a mechanical test would be needed to confirm these results.

Up to this point, we have fit the model assuming single slip and ignoring lattice rotation. For the given sample orientation, there is no resolved shear stress on the basal slip systems, and the resolved shear stress on the remaining two prismatic slip systems is

Table 1 Some possible prismatic slip modeling parameters for GaN

v_o ($\times 10^3$ m/s)	Q^p (eV)	n	$\hat{\tau}_f^p$ (MPa)	g_1^p ($\times 10^{-6}$)	g_2^p ($\times 10^3$)	g_3^p ($\times 10^{-5}$)
0.1	2.76	2.83	44.1	3.3	3.4	2.8
10	3.41	3.34	45.3	3.9	6.8	18.2

Table 2 Optimal prismatic slip modeling parameters for GaN with $v_o = 10^3$ m/s

Model	Q^p (eV)	n	$\hat{\tau}_f^p$ (MPa)	g_1^p ($\times 10^{-6}$)	g_2^p ($\times 10^3$)	g_3^p ($\times 10^{-5}$)
A	3.10	3.09	44.8	3.6	4.5	7.7
B	2.02	3.78	52.2	0.5	0.7	3.2

Model A assumes Eq. (20) and model B assumes Eq. (21) for the power law.

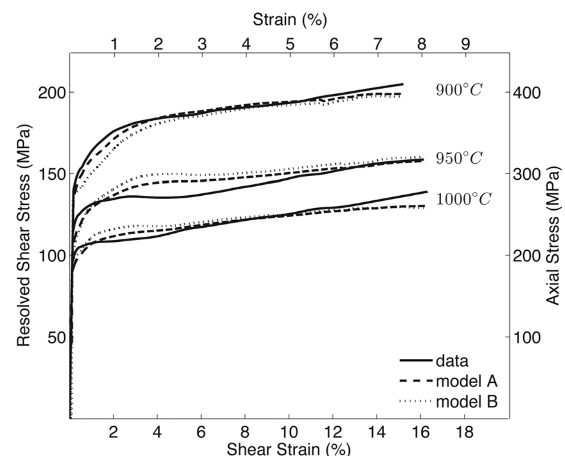

Fig. 5 Stress–strain curves from proposed model for GaN versus experiment data [9], at temperatures of 900, 950, and 1000 °C. Model A assumes Eq. (20) and model B assumes Eq. (21).

Downloaded From: http://materialstechnology.asmedigitalcollection.asme.org/ on 03/17/2016 Terms of Use: http://www.asme.org/about-asme/terms-of-use

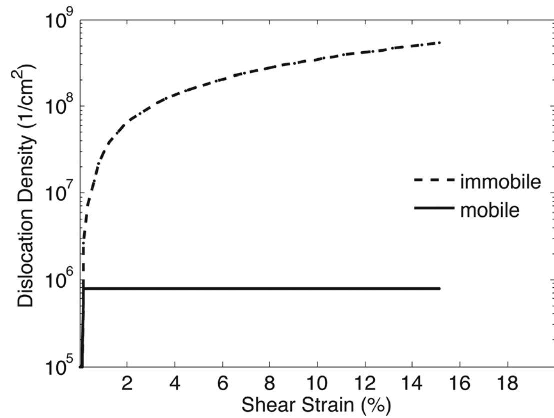

Fig. 6 Computed dislocation density for the experiment [9], at temperatures of 900, 950, and 1000 °C

$$|\tau^2| = |\tau^3| = \frac{1}{4}|\sigma_{22}| = \frac{1}{2}|\tau^1| \tag{33}$$

where $\alpha = 1$ refers to the slip system oriented at 45 deg to the loading direction and $\alpha = 2$ and $\alpha = 3$ are the slip systems oriented 60 deg in either direction from the $\alpha = 1$ slip system, with slip planes aligned with a_2 and a_1 in Fig. 1. For the optimal parameters listed in Table 2 and assuming the power law in Eq. (20), the rate of shearing on slip systems 2 and 3 is always less than 1.6% that on slip system 1, and, for most of the test, no slip is predicted on slip systems 2 and 3. Thus, the single slip approximation is valid.

As the deformation proceeds, the lattice will rotate according to Eq. (17). Since the sample is fixed between the platens during the compression test, the sample is not expected to rotate, i.e., $\dot{w}_{ij} = 0$, and thus for this single slip case we have

$$\dot{R}_{il}R_{jl} = -\dot{w}^p_{ij} = -\frac{1}{2}\dot{\gamma}R_{ik}(\bar{s}_k\bar{m}_l - \bar{s}_l\bar{m}_k)R_{jl}$$

or

$$\dot{R}_{il} = -\frac{1}{2}\dot{\gamma}R_{ik}(\bar{s}_k\bar{m}_l - \bar{s}_l\bar{m}_k) \tag{34}$$

Integrating Eq. (34), using an exponential update [48] to solve for the rotation R_{il} that defines the lattice orientation, we find that the lattice rotates 4.6 deg counterclockwise, relative to the orientation shown in Fig. 1, during the test. Thus, the primary active slip plane ends up inclined by 49.6 deg from the compression axis. For this orientation, the resolved shear stress and rate of shearing on the primary slip system are related to the applied compressive stress and plastic strain rate

$$|\tau| = 0.4936|\sigma_{22}|, \quad |\dot{\gamma}| = 2.026|\dot{\varepsilon}^p_{22}| \tag{35}$$

as compared to coefficients of 0.5 and 2, respectively, at the beginning of the test. Thus, the lattice rotation represents part of the observed hardening, but the error in neglecting the lattice rotation is less than 1.5%.

Finally, estimates for parameters for basal slip are made based on the molecular dynamics dislocation mobility study by Weingarten and Chung [38]. That study models a pure edge dislocation without boundary effects. They find similar mobilities for the basal and prismatic slip systems, with slightly higher mobility on the basal plane. GaN has a lattice ratio of $c/a = 1.63$, which is the ratio for ideal packing, and, thus, slip on the basal and prismatic slip systems is expected to be equal. The strain rate sensitivity and activation energies were found to be nearly identical on the basal and prismatic slip systems, and the stress level required to move a dislocation at a given velocity on the basal plane was found to be about 70% of that required on the prismatic slip system. No information on dislocation density evolution is available from that study. Based on this limited information, the parameters for basal slip are estimated to be the same as that for prismatic slip except $\hat{\tau}^b_f \approx 0.7\hat{\tau}^p_f \approx 30$ MPa. Experimental data from a single crystal oriented for basal slip is required for a more accurate estimate of the model parameters.

6 Discussion and Conclusions

The constitutive model developed in this work provides a framework for modeling the thermal–mechanical response of bulk wurtzite single-crystals at elevated temperatures. Model parameters for prismatic and basal slip in GaN are defined. The degree of confidence in the prismatic slip parameters is much higher than that for basal slip as the prismatic slip parameters are found by fitting available single-slip experimental data. The model could be further refined if additional data becomes available. Most useful would be data for basal slip, information on dislocation density both before and after the test, and data over a wider temperature range. The model may be used to predict both the stress state and the dislocation density under growth conditions, which are both associated with the crystal quality as excess stress may lead to cracking and a high dislocation density adversely affects device performance.

Acknowledgment

This work was supported by the National Science Foundation under Grant No. CMMI-0928556. The authors acknowledge many helpful discussions with Dr. R. Bondokov and Dr. L. Schowalter of Crystal IS, Inc.

References

[1] Strite, S., and Morkoc, H., 1992, "GaN, AlN, and InN: A Review," J. Vac. Sci. Technol. B, **10**(4), pp. 1237–1266.

[2] Nakamura, S., 1997, "First III-V-Nitride-Based Violet Laser Diodes," J. Cryst. Growth, **170**(1-4), pp. 11–15.

[3] Wang, J., Ryu, H.-B., Park, M.-S., Lee, W.-J., Choi, Y.-J., and Lee, H.-Y., 2013, "Epitaxy of GaN on Si(111) Substrate by the Hydride Vapor Phase Epitaxy Method," J. Cryst. Growth, **370**, pp. 249–253.

[4] Motoki, K., Okahisa, T., Nakahata, S., Matsumoto, N., Kimura, H., Kasai, H., Takemoto, K., Uematsu, K., Ueno, M., Kumagai, Y., Koukitu, A., and Seki, H., 2002, "Growth and Characterization of Freestanding GaN Substrates," J. Cryst. Growth, **237**(2), pp. 912–921.

[5] Andre, Y., Trassoudaine, A., Tourret, J., Cadoret, R., Gil, E., Castelluci, D., Aoude, O., and Disseix, P., 2007, "Low Dislocation Density High-Quality Thick Hydride Vapour Phase Epitaxy (HVPE) GaN Layers," J. Cryst. Growth, **306**(1), pp. 86–93.

[6] Yoshikawa, A., Ohshima, E., Fukuda, T., Tsuji, H., and Oshima, K., 2004, "Crystal Growth of GaN by Ammonothermal Method," J. Cryst. Growth, **260**(1), pp. 67–72.

[7] Dwiliński, R., Doradziński, R., Garczyński, J., Sierzputowski, L., Puchalski, A., Kanbara, Y., Yagi, K., Minakuchi, H., and Hayashi, H., 2008, "Excellent Crystallinity of Truly Bulk Ammonothermal GaN," J. Cryst. Growth, **310**(17), pp. 3911–3916.

[8] Dwiliński, R., Doradziński, R., Garczyński, J., Sierzputowski, L., Kucharski, R., Zajac, M., Rudziński, M., Kudrawiec, R., Strupiński, W., and Misiewicz, J., 2011, "Ammonothermal GaN Substrates: Growth Accomplishments and Applications," Phys. Status Solidi, **208**(7), pp. 1489–1493.

[9] Yonenaga, I., and Motoki, K., 2001, "Yield Strength and Dislocation Mobility in Plastically Deformed Bulk Single-Crystal GaN," J. Appl. Phys., **90**(12), pp. 6539–6541.

[10] Leszczynski, M., Suski, T., Teisseyre, H., Perlin, P., Grzegory, I., Jun, J., Porowski, S., and Moustakas, T. D., 1994, "Thermal Expansion of Gallium Nitride," J. Appl. Phys., **76**(8), pp. 4909–4911.

[11] Reeber, R. R., and Wang, K., 2000, "Lattice Parameters and Thermal Expansion of Important Semiconductors and Their Substrates," MRS Proc., **622**(1), p. T6.35.1.

[12] Wang, H.-Y., Hui, X., Huang, T.-T., and Deng, C.-S., 2008, "Thermodynamics of Wurtzite GaN From First-Principle Calculation," Eur. Phys. J. B, **62**(1), pp. 39–43.

[13] Yadav, R. R., and Pandey, D. K., 2006, "Ultrasonic Characterisation of Gallium Nitride," Mater. Res. Innov., **10**(4), pp. 402–407.

[14] Reeber, R. R., and Wang, K., 2001, "High Temperature Elastic Constant Prediction of Some Group III-Nitrides," MRS Internet J. Nitride Semicond. Res., **6**, p. e3.

Downloaded From: http://materialstechnology.asmedigitalcollection.asme.org/ on 03/17/2016 Terms of Use: http://www.asme.org/about-asme/terms-of-use

[15] Fujikane, M., Yokogawa, T., Nagao, S., and Nowak, R., 2012, "Nanoindentation Study on Insight of Plasticity Related to Dislocation Density and Crystal Orientation in GaN," Appl. Phys. Lett., **101**(20), p. 201901.
[16] Lu, J.-Y., Ren, H., Deng, D.-M., Wang, Y., Chen, K. J., Lau, K.-M., and Zhang, T.-Y., 2012, "Thermally Activated Pop-In and Indentation Size Effects in GaN Films," J. Phys. D, **45**(8), p. 085301.
[17] Yonenaga, I., Hoshi, T., and Usui, A., 2000, "Hardness of Bulk Single-Crystal Gallium Nitride at High Temperatures," Jpn. J. Appl. Phys., **39**(3A/B), pp. L200–L201.
[18] Lloyd, S. J., Molina-Aldareguia, J. M., and Clegg, W. J., 2001, "Deformation Under Nanoindents in Si, Ge, and GaAs Examined Through Transmission Electron Microscopy," J. Mater. Res., **16**(12), pp. 3347–3350.
[19] Wheeler, J. M., Niederberger, C., Tessarek, C., Christiansen, S., and Michler, J., 2013, "Extraction of Plasticity Parameters of GaN With High Temperature, In Situ Micro-Compression," Int. J. Plast., **40**, pp. 140–151.
[20] Alexander, H., and Haasen, P., 1968, "Dislocations in the Diamond Structure," *Advances in Solid State Physics*, Vol. 22, F. Sietz, D. Turnbull, and H. Ehrenreich, eds., Academic Press, New York, pp. 27–158.
[21] Yonenaga, I., and Sumino, K., 1978, "Dislocation Dynamics in the Plastic Deformation of Silicon Crystals," Phys. Status Solidi A, **50**(2), pp. 685–693.
[22] Yonenaga, I., 1997, "Mechanical Properties and Dislocation Dynamics in III-V Compounds," Journal de Physique III, **7**(7), pp. 1435–1450.
[23] Garofalo, F., 1963.,"Empirical Relation Defining Stress Dependence of Minimum Creep Rate in Metals," Metall. Soc. AIME, **227**(2), pp. 351–356.
[24] Moosbrugger, J. C., 1995, "Continuum Slip Viscoplasticity With the Haasen Constitutive Model: Application to CdTe Single Crystal Inelasticity," Int. J. Plast., **11**(7), pp. 799–826.
[25] Kalan, R. J., and Maniatty, A. M., 2001, "Micromechanical Constitutive Relations for Modeling the Bulk Growth of Single Crystal InP," J. Cryst. Growth, **233**(4), pp. 645–659.
[26] Cochard, J., Yonenaga, I., Gouttebroze, S., M'Hamdi, M., and Zhang, Z. L., 2010, "Constitutive Modeling of Intrinsic Silicon Monocrystals in Easy Glide," J. Appl. Phys., **107**(3), p. 033512.
[27] Bower, A. F., 2010, *Applied Mechanics of Solids*, CRC Press, Boca Raton, FL.
[28] Orowan, E., 1940, "Problems of Plastic Gliding," Proc. Phys. Soc. London, **52**(1), pp. 8–22.
[29] Frost, H. J., and Ashby, M. F., 1982, *Deformation-Mechanism Maps*, Pergamon Press, New York.
[30] Utsumi, W., Saitoh, H., Kaneko, H., Watanuki, T., Aoki, K., and Shimomura, O., 2003, "Congruent Melting of Gallium Nitride at 6 GPa and Its Application to Single-Crystal Growth," Nat. Mater., **2**(11), pp. 735–738.
[31] Maniatty, A. M., Dawson, P. R., and Lee, Y. S., 1992, "A Time Integration Algorithm for Elasto-Viscoplastic Cubic Crystals Applied to Modeling Polycrystalline Deformation," Int. J. Numer. Methods Eng., **35**(8), pp. 1565–1588.
[32] Hutchinson, J. W., 1976, "Bounds and Self-Consistent Estimates for Creep of Polycrystalline Materials," Proc. R. Soc. A, **348**(1652), pp. 101–127.
[33] Johnston, W. G., and Gilman, J. J., 1959, "Dislocation Velocities, Dislocation Densities, and Plastic Flow in Lithium Fluoride Crystals," J. Appl. Phys., **30**(2), pp. 129–143.
[34] Dew-Hughes, D., 1961, "Dislocations and Plastic Flow in Germanium," IBM J. Res. Dev., **5**(4), pp. 279–286.
[35] Peissker, E., Haasen, P., and Alexander, H., 1962, "Anisotropic Plastic Deformation of Indium Antimonide," Philos. Mag., **7**(80), pp. 1279–1303.
[36] Kubin, L. P., and Estrin, Y., 1990, "Evolution for Dislocation Densities and the Critical Conditions for the Portevin–Le Chatelier Effect," Acta Metall. Mater., **38**(5), pp. 697–708.
[37] Huang, J., Xu, K., Gong, X. J., Wang, J. F., Fan, Y. M., Liu, J. Q., Zeng, X. H., Ren, G. Q., Zhou, T. F., and Yang, H., 2011, "Dislocation Cross-Slip in GaN Single Crystals Under Nanoindentation," Appl. Phys. Lett., **98**(22), p. 221906.
[38] Weingarten, N. S., and Chung, P. W., 2013, "A-Type Edge Dislocation Mobility in Wurtzite GaN Using Molecular Dynamics," Scr. Mater., **69**(4), pp. 311–314.
[39] Dasilva, Y. A. R., Ruterana, P., Lahourcade, L., Monroy, E., and Nataf, G., 2010, "Extended Crystallographic Defects in Gallium Nitride," Mater. Sci. Forum, **644**, pp. 117–122.
[40] Bai, J., Dudley, M., Raghothamachar, B., Gouma, P., Skromme, B. J., Chen, L., Hartlieb, P. J., Michaels, E., and Kolis, J. W., 2004, "Correlated Structural and Optical Characterization of Ammonothermally Grown Bulk GaN," Appl. Phys. Lett., **84**(17), pp. 3289–3291.
[41] Beyerlein, I. J., and Tomé, C. N., 2008, "A Dislocation-Based Constitutive Law for Pure Zr Including Temperature Effects," Int. J. Plast., **24**(5), pp. 867–895.
[42] Hosford, W. F., 1993, *The Mechanics of Crystals and Textured Polycrystals*, Oxford University Press, New York.
[43] Patel, J. R., and Chaudhuri, A. R., 1963, "Macroscopic Plastic Properties of Dislocation-Free Germanium and Other Semiconductor Crystals. I. Yield Behavior," J. Appl. Phys., **34**(9), p. 2788.
[44] Yonenaga, I., and Sumino, K., 1993, "Effects of Dopants on Dynamic Behavior of Dislocations and Mechanical Strength in InP," J. Appl. Phys., **74**(2), pp. 917–924.
[45] Reppich, B., Reiger, K., and Muller, G., 1990, "Dynamische Verformung von InP-Einkristallen Bei Hochsten Temperaturen Mittels Liquid-Encapsulation (LE)-Technik," Z. Metallkd., **81**, pp. 166–173.
[46] Samant, A. V., Zhou, W. L., and Pirouz, P., 1998, "Effect of Test Temperature and Strain Rate on the Yield Stress of Monocrystalline 6H-SiC," Phys. Status Solidi A, **166**(1), pp. 155–169.
[47] Anderssen, R., and Hegland, M., 1999, "For Numerical Differentiation, Dimensionality Can Be a Blessing!" Math. Comput., **68**(227), pp. 1121–1142.
[48] Simo, J. C., and Hughes, T. J. R., 1998, *Computational Inelasticity*, Springer, New York.

Downloaded From: http://materialstechnology.asmedigitalcollection.asme.org/ on 03/17/2016 Terms of Use: http://www.asme.org/about-asme/terms-of-use